Carbon Isotope Constraints on the Deglacial CO_2 Rise from Ice Cores

Jochen Schmitt,[1,2]* Robert Schneider,[1] Joachim Elsig,[1] Daiana Leuenberger,[1] Anna Lourantou,[3]† Jérôme Chappellaz,[3] Peter Köhler,[2] Fortunat Joos,[1] Thomas F. Stocker,[1] Markus Leuenberger,[1] Hubertus Fischer[1,2]

The stable carbon isotope ratio of atmospheric CO_2 ($\delta^{13}C_{atm}$) is a key parameter in deciphering past carbon cycle changes. Here we present $\delta^{13}C_{atm}$ data for the past 24,000 years derived from three independent records from two Antarctic ice cores. We conclude that a pronounced 0.3 per mil decrease in $\delta^{13}C_{atm}$ during the early deglaciation can be best explained by upwelling of old, carbon-enriched waters in the Southern Ocean. Later in the deglaciation, regrowth of the terrestrial biosphere, changes in sea surface temperature, and ocean circulation governed the $\delta^{13}C_{atm}$ evolution. During the Last Glacial Maximum, $\delta^{13}C_{atm}$ and atmospheric CO_2 concentration were essentially constant, which suggests that the carbon cycle was in dynamic equilibrium and that the net transfer of carbon to the deep ocean had occurred before then.

During the past 800,000 years, atmospheric CO_2 concentrations have varied in close relation to Antarctic temperatures (*1*, *2*) and the general waxing and waning of continental ice sheets. In particular, CO_2 rose from a stable level of 190 parts per million by volume (ppmv) during the Last Glacial Maximum to about 280 ppmv in preindustrial times, showing pronounced differences in atmospheric CO_2 rates of change in the course of the last glacial-interglacial transition (*3*). Many processes have been invoked in attempts to explain these CO_2 variations, but it has become evident that none of these mechanisms alone can account for the 90-ppmv increase in atmospheric CO_2. A combination of processes must have been operating (*4*, *5*), with the sequence of events, their durations, and their amplitudes being crucial. However, a unique solution to the deglacial carbon cycle changes has not yet been found.

In this respect, high-resolution and precise $\delta^{13}C_{atm}$ records from Antarctic ice cores are needed to better constrain the evolution of carbon cycle changes during the last deglaciation. On millennial time scales, $\delta^{13}C_{atm}$ is primarily influenced by the $\delta^{13}C$ of dissolved inorganic carbon (DIC) ($\delta^{13}C_{DIC}$) and by sea surface temperature (SST), which controls the isotopic fractionation during air/sea gas exchange. The continuous rain of isotopically light organic material to the interior of the ocean draws carbon down from the surface layer to intermediate and deep waters, where the organic carbon is remineralized. Consequently, a vertical $\delta^{13}C_{DIC}$ gradient is established, controlled by the interplay of the ocean circulation with this so-called "biological pump." The more intense the circulation, the smaller the gradients are for $\delta^{13}C_{DIC}$, DIC, oxygen, and nutrients. Superimposed on these marine carbon cycle processes are climate-induced changes in terrestrial biosphere carbon storage, which result in a net change in the carbon isotopic composition of the ocean-atmosphere system. On orbital time scales, weathering and sedimentation of $CaCO_3$ affect $\delta^{13}C_{DIC}$, $\delta^{13}C_{atm}$, and the atmospheric CO_2 concentration as well.

Until recently (*6*), analytical constraints represented a fundamental limitation on the utility of $\delta^{13}C_{atm}$ ice core records (*7*, *8*). Here, we provide evidence (Fig. 1) about possible causes of carbon cycle changes with measurements of $\delta^{13}C_{atm}$ from two Antarctic ice cores—EPICA (European Project for Ice Coring in Antarctica) Dome C and Talos Dome—performed with three independent methods in two different labs (referred to as Bern sublimation, Bern cracker, and Grenoble mill data) (*6*, *9*). One of our records is based on a novel sublimation method (*10*) that avoids the effects associated with incomplete gas extraction and thus yields more precise results (see supplementary materials). A stringent residual analysis of the three data sets shows virtually no offset between the two Bern data sets and only a small systematic offset between the Bern and Grenoble data of 0.16 per mil (‰), which can be explained by a method-dependent systematic fractionation. After correction of this offset, we used an error-weighted Monte Carlo bootstrap approach to combine the three $\delta^{13}C_{atm}$ records over the past 24,000 years. This method showed that all three data sets are essentially compatible within their analytical uncertainties. Although all our conclusions are supported by the individual records, we combined all three data sets to make full use of the resolution and precision of the data. The final data set consists of 201 individual measurements, each reflecting typically two to four replicates and with an analytical 1σ error between 0.04 and 0.12‰. Because the resulting Monte Carlo average (MCA) removes most of the analytical uncertainties, it contains less high-frequency variability relative to the raw data. This is in line with the centennial-scale low-pass filtering inherent in the firn densification process, which gradually encloses air bubbles, finally leading to the atmospheric archive. Accordingly, the retained variability can be regarded as the signal most representative of millennial $\delta^{13}C_{atm}$ changes (see supplementary materials for details regarding the MCA and its uncertainty).

Our $\delta^{13}C_{atm}$ data are in good agreement with previously published lower-resolution records (*6*, *9*). Our record shows a very stable level between 24,000 and ~19,000 years before present (B.P., where present is defined as 1950), with an average $\delta^{13}C_{atm}$ of −6.45‰ (tables S1 and S2), similar to the −6.35‰ of the Late Holocene (Fig. 2B). Given the fact that a large set of environmental parameters such as atmospheric CO_2, global SST, terrestrial carbon storage, and ocean circulation have varied between the LGM and the Late Holocene, almost identical $\delta^{13}C_{atm}$ values indicate that opposing effects must have offset each other (*11*). This becomes clear if we look at three first-order effects on $\delta^{13}C_{atm}$: A SST rise of 1 K translates into a 0.1‰ increase in $\delta^{13}C_{atm}$, due to temperature-dependent fractionation between atmospheric CO_2 and marine DIC species (*12*). The assumption of a global LGM-to-Holocene SST rise of 3 K would result in about 0.3‰ higher $\delta^{13}C_{atm}$ for the Holocene, provided that SST distribution and CO_2 gross flux exchange patterns remained constant. This effect is further augmented by the uptake of isotopically light carbon by the land biosphere and is counterbalanced by the smaller vertical gradient in $\delta^{13}C_{DIC}$ in the Holocene ocean, supported by marine data (*13*). The fact that both $\delta^{13}C_{atm}$ and CO_2 show little variation from 24,000 to 19,000 years B.P. points to the carbon cycle being essentially in dynamic equilibrium at that time. As can also be seen in Fig. 2, the climate variations related to Heinrich stadial 2 (HS2) and Dansgaard-Oeschger event 2 (DO2) had little effect on the global carbon cycle during this time interval. However, given the opposing trends for reconstructed atmospheric $\Delta^{14}C$ ($\Delta^{14}C_{atm}$) (*14*, *15*) and the expected $\Delta^{14}C_{atm}$ evolution (*16*) based on variations in ^{14}C production rate (*17*, *18*), the global ^{14}C budget was not balanced (Fig. 2A).

After a very small increase in $\delta^{13}C_{atm}$ at the very end of the glacial, a sharp drop in $\delta^{13}C_{atm}$ starting at 17,500 years B.P. parallels the onset of increasing atmospheric CO_2. Taken at face value, the small local maximum would point to an early SST rise that preceded the onset of the CO_2 increase. When we apply a crude SST correction to our $\delta^{13}C_{atm}$ data, on the basis of a global estimate of SST temperature changes during the transition (see supplementary materials), this $\delta^{13}C_{atm}$ increase vanishes (Fig. 2B). Note, however, that this 0.06‰ excursion is within the uncertainties of our data and that other effects could also lead to this small enrichment in $\delta^{13}C_{atm}$. The 0.3‰ drop in $\delta^{13}C_{atm}$ after the onset of the transition at 17,500 years B.P. is accompanied by

[1]Climate and Environmental Physics, Physics Institute, and Oeschger Centre for Climate Change Research, University of Bern, CH-3012 Bern, Switzerland. [2]Alfred Wegener Institute for Polar and Marine Research, 27570 Bremerhaven, Germany. [3]UJF–Grenoble 1/CNRS, Laboratoire de Glaciologie et Géophysique de l'Environnement (LGGE) UMR 5183, 38041 Grenoble, France.

*To whom correspondence should be addressed. E-mail: schmitt@climate.unibe.ch

†Present address: Laboratoire d'Océanographie et du Climat (LOCEAN), Institut Pierre Simon Laplace, Université P. et M. Curie, 75005 Paris, France.

a CO_2 increase of about 35 ppmv and a 190‰ drop in $\Delta^{14}C_{atm}$ (*19*), which has been attributed to a release of old carbon from the deep ocean. This coeval drop in $\delta^{13}C_{atm}$ and $\Delta^{14}C_{atm}$ during the so-called "mystery interval," 17,500 to 14,000 years B.P. (*19*), is arguably the most enigmatic carbon cycle change in the course of the transition (see below).

After the broad $\delta^{13}C_{atm}$ minimum is reached at about 16,000 years B.P., $\delta^{13}C_{atm}$ increases slightly by 0.1‰ during the pronounced Bølling-Allerød warming. Other than circulation changes in the Southern Ocean (*20*), the regrowth of the terrestrial biosphere in the northern hemisphere could contribute to this increase in $\delta^{13}C_{atm}$ (*4*). However, because the SST-corrected $\delta^{13}C$ evolution (Fig. 2B) does not show any increase, a robust process attribution requires precisely dated SST reconstructions and transient carbon cycle modeling.

An almost linear rise by 0.06‰ per 1000 years follows the second $\delta^{13}C_{atm}$ minimum at 12,200 years B.P., leading to maximum values of −6.33‰ at around 6000 years B.P. This rise might be largely explained by the continuing regrowth of the terrestrial biosphere (*21*), in concert with smaller contributions from SST warming and changes in circulation and export production (*9*, *22*). From this mid-Holocene maximum, $\delta^{13}C_{atm}$ values decline slightly to reach values of −6.35‰ at 500 years B.P., as previously reported (*6*).

As mentioned above, the carbon cycle changes during the mystery interval have been a matter of intense debate (*19*, *20*, *23*). Our high-resolution $\delta^{13}C_{atm}$ record, together with other records of carbon cycle changes and insights from models, may help to constrain hypotheses put forward to explain the mystery interval. The rise in CO_2 and the decline in $\delta^{13}C_{atm}$ and $\Delta^{14}C_{atm}$ between 17,000 and 15,000 years B.P. fit the concept of bringing DIC-rich waters with old carbon into exchange with the atmosphere. Indicative ^{14}C signals of upwelling of old, CO_2-enriched deep water were found in Pacific intermediate waters (*24*), but other studies (*23*) ruled out such old water in the northeast Pacific, and evidence for a ^{14}C-depleted glacial deep ocean remains elusive (*19*, *23*, *25*). These $\Delta^{14}C$ studies were usually confronted with variable reservoir age between benthic and planktonic foraminifera. A study using deep sea corals now circumvents this problem by applying absolute U-Th dating and shows that the deep glacial Southern Ocean indeed ventilated its ^{14}C-depleted reservoir during the mystery interval (*26*).

The constant $\delta^{13}C_{atm}$ values during the late glacial indicate that the buildup of such an old, DIC-rich reservoir must have occurred before 24,000 years B.P. A large number of records mark the start of the deglaciation around 17,000 years B.P. (Fig. 2). Within the uncertainty in marine and ice core age scales, the CO_2 increase, the pronounced $\Delta^{14}C_{atm}$ drop (*15*), the resumption of vigorous Southern Ocean upwelling as recorded in intense deposition of biogenic opal (*20*), and the launch of ice-rafted debris layers at the beginning of the Heinrich 1 stadial (*27*) all occurred simultaneously.

Our $\delta^{13}C_{atm}$ record shows its largest deviation of 0.3‰—that is, the entire $\delta^{13}C_{atm}$ decrease from the LGM to the Preboreal—within the first 2000 years after the start of the deglaciation. Within the same 2000-year interval, CO_2 rose from 190 ppmv to 220 ppmv (i.e., only 35% of the LGM-Preboreal rise). Together with the trend reversal in $\delta^{13}C_{atm}$ toward the end of the mystery interval, this indicates that only a fraction of the glacial/interglacial CO_2 increase can be explained by an intensification of deep ocean ventilation bringing isotopically depleted and carbon-rich water to the surface of the Southern Ocean. Our new, high-resolution $\delta^{13}C_{atm}$ data constrain this release of isotopically depleted carbon from the deep ocean to the atmosphere to the period 17,400 to 15,000 years B.P. This interpretation of the proxy records is quantitatively in line with dynamical ocean model results that link deep ocean ventilation, atmospheric CO_2, $\delta^{13}C_{atm}$, $\delta^{13}C_{DIC}$, opal burial, and radiocarbon (*28*).

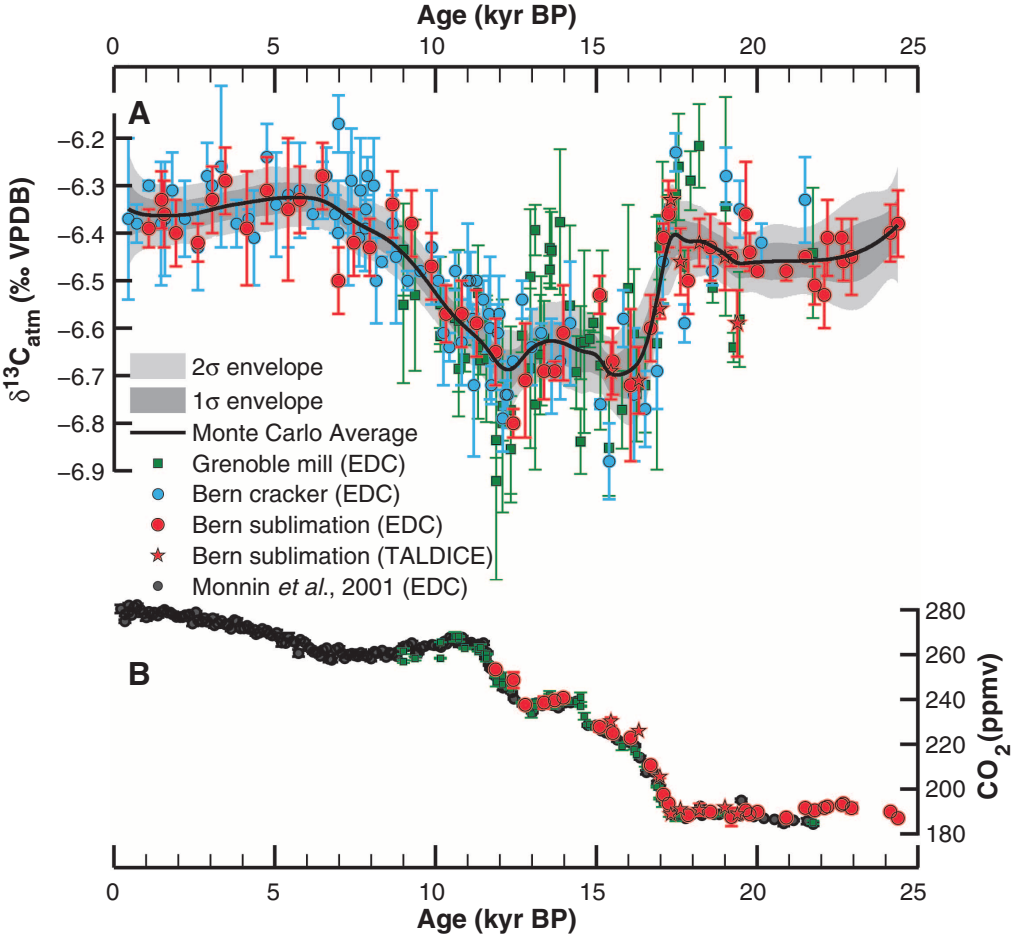

Fig. 1. Ice core reconstructions of atmospheric $\delta^{13}C$ and CO_2 concentration covering the past 24,000 years (24 kyr). (**A**) $\delta^{13}C_{atm}$ of atmospheric CO_2 measured with three different methods on two different ice core drill sites. Blue circles, Bern cracker data; green squares, Grenoble mill data (*9*) after offset correction; red circles, Bern sublimation data. Red stars indicate values from the sublimation method but measured on Talos Dome Ice Core (TALDICE). Error bars represent SD of replicate measurements where available and the mean SD for single measurements. The black line is the result of 4000 Monte Carlo simulations representing an error-weighted average of the different $\delta^{13}C_{atm}$ data sets. The light and dark shaded areas represent the 2σ and 1σ error envelope around the Monte Carlo average (MCA). (**B**) CO_2 concentration. Black circles represent earlier measurements on EPICA Dome C (EDC) (*3*); other symbols are the same as in (A). All ice core records are plotted on a synchronized age scale (*32*).

Alternative hypotheses (*29*, *30*) invoking the release of old carbon from permafrost or carbon locked under continental ice sheets are unlikely to explain the carbon cycle changes in the mystery interval, because the amount of terrestrial carbon needed to account for the ^{14}C drop is very large [about 5000 Gt (*25*)] and would conflict with the moderate 30-ppmv rise in atmospheric CO_2. Moreover, it would lead to an overall decline in $\delta^{13}C_{DIC}$, which is not observed in benthic foraminifera in the deep ocean (*13*, *22*). Also, a carbonate dissolution event at the sea floor that would have to accompany such a large terrestrial carbon release into the atmosphere-ocean system is not imprinted in the deglacial marine $CaCO_3$ record (*31*).

Consequently, even though the search for an extremely ^{14}C-depleted deep water mass in marine records has so far not been successful (*23*) and might not even be essential to explain the $\Delta^{14}C_{atm}$ anomaly (*26*), the release of carbon from the deep ocean remains the most plausible scenario to explain the early deglacial drop in our new $\delta^{13}C_{atm}$ record. Furthermore, model results suggest that a $\delta^{13}C_{atm}$ decrease of 0.3‰ and a CO_2 increase of about 30 ppmv can be accommodated by relatively small (about 20‰) and spatially complex changes in deep ocean $\Delta^{14}C$ (*28*). These changes may remain undetected in attempts to use benthic foraminifera as clues to the location of old abyssal water (*19*, *25*). However, such changes are also too small to explain the reconstructed $\Delta^{14}C_{atm}$ decline during the mystery interval. Because of these considerations, the currently available marine and ice core information cannot be reconciled with the atmospheric radiocarbon record in a straightforward manner. One possible way to resolve this issue is to consider the possibility of a larger change in ^{14}C production between the Holocene and the glacial, and to work toward independent verification of the $\Delta^{14}C_{atm}$ history.

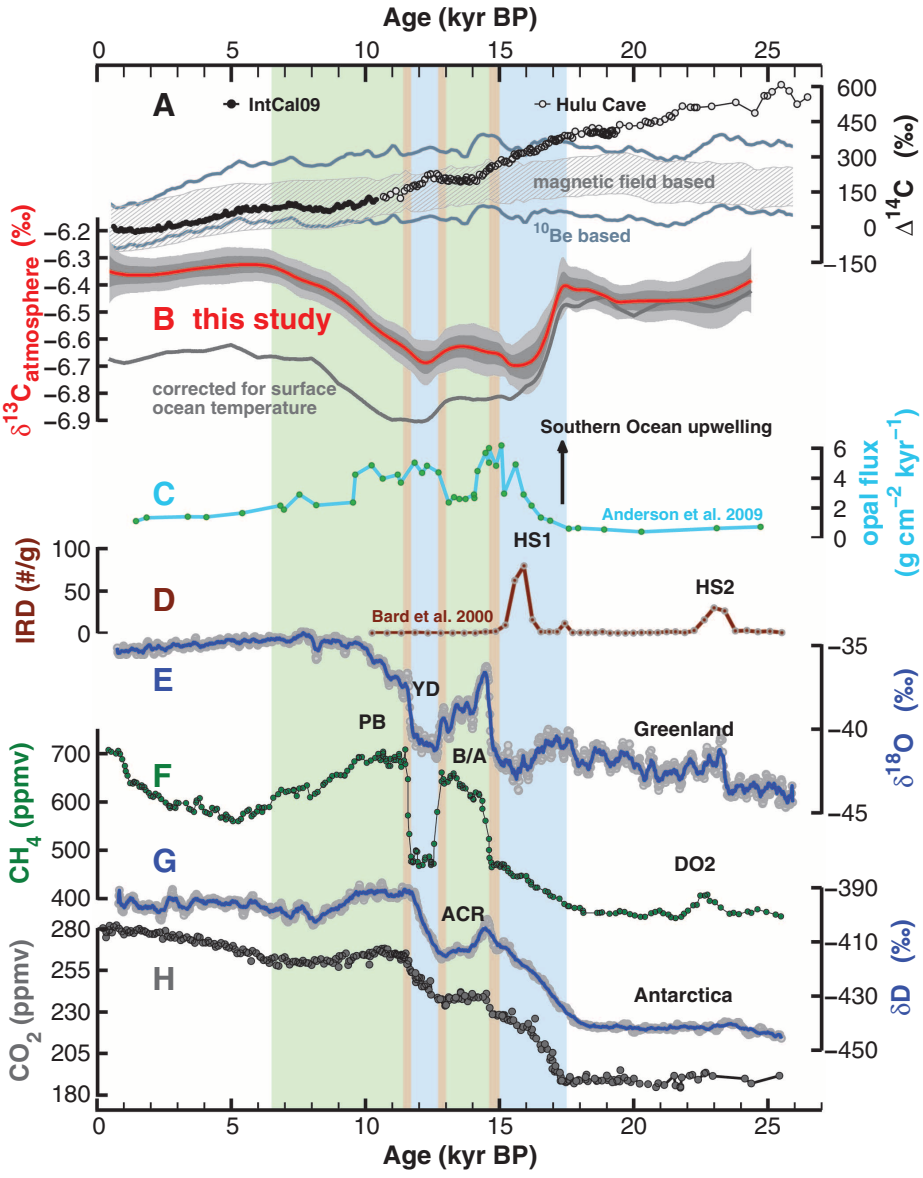

Fig. 2. Ice core reconstructions and marine records illustrating the evolution of major components of the Earth climate system over the past 24,000 years. (**A**) Reconstructed $\Delta^{14}C_{atm}$ from IntCal09 (*14*) and the ^{230}Th-dated Hulu Cave $\Delta^{14}C_{atm}$ record (*15*) compared with modeled (*16*) $\Delta^{14}C_{atm}$, assuming a constant carbon cycle under preindustrial conditions but considering temporal changes in ^{14}C production [based on ^{10}Be (*18*), upper and lower estimates (gray lines), or based on paleomagnetic field intensity (*17*), hatched area]. (**B**) Monte Carlo average (this study) of the evolution of $\delta^{13}C_{atm}$ before SST correction (red line represents the MCA; 2σ and 1σ envelopes are in gray) and after SST correction (gray line). (**C**) Opal flux in the Southern Ocean as a proxy for local upwelling (*20*). (**D**) Record of ice-rafted debris (IRD) in the North Atlantic associated with Heinrich stadials HS1 and HS2 (*27*). (**E**) Greenland temperature proxy $\delta^{18}O$ (*33*). (**F**) Reconstructed atmospheric CH_4 concentration (*34*). (**G**) Antarctic temperature proxy δD from the EDC ice core (*35*). (**H**) Compilation of reconstructed CO_2 shown in Fig. 1B. Green bars indicate intervals with a strong net terrestrial carbon buildup; blue bars indicate intervals where sequestered deep ocean CO_2 was released back to the atmosphere. Note that ice core records are plotted on a synchronized age scale (*32*), whereas other records are plotted on their individual age scales. PB, Preboreal; YD, Younger Dryas; B/A, Bølling-Allerød warming; DO2, Dansgaard-Oeschger event 2; ACR, Antarctic Cold Reversal.

References and Notes

1. D. Lüthi *et al.*, *Nature* **453**, 379 (2008).
2. H. Fischer *et al.*, *Quat. Sci. Rev.* **29**, 193 (2010).
3. E. Monnin *et al.*, *Science* **291**, 112 (2001).
4. P. Köhler, H. Fischer, G. Munhoven, R. E. Zeebe, *Global Biogeochem. Cycles* **19**, GB4020 (2005).
5. D. M. Sigman, M. P. Hain, G. H. Haug, *Nature* **466**, 47 (2010).
6. J. Elsig *et al.*, *Nature* **461**, 507 (2009).
7. H. J. Smith, H. Fischer, M. Wahlen, D. Mastroianni, B. Deck, *Nature* **400**, 248 (1999).
8. M. Leuenberger, U. Siegenthaler, C. C. Langway, *Nature* **357**, 488 (1992).
9. A. Lourantou *et al.*, *Global Biogeochem. Cycles* **24**, GB2015 (2010).
10. J. Schmitt, R. Schneider, H. Fischer, *Atmos. Meas. Tech.* **4**, 1445 (2011).
11. P. Köhler, H. Fischer, J. Schmitt, *Paleoceanography* **25**, PA1213 (2010).
12. J. Zhang, P. D. Quay, D. O. Wilbur, *Geochim. Cosmochim. Acta* **59**, 107 (1995).
13. K. I. C. Oliver *et al.*, *Clim. Past* **6**, 645 (2010).
14. P. J. Reimer *et al.*, *Radiocarbon* **51**, 1111 (2009).
15. J. Southon, A. L. Noronha, H. Cheng, R. L. Edwards, Y. Wang, *Quat. Sci. Rev.* **33**, 32 (2012).
16. P. Köhler, R. Muscheler, H. Fischer, *Geochem. Geophys. Geosyst.* **7**, Q11N06 (2006).
17. C. Laj, C. Kissel, J. Beer, in *Timescales of the Paleomagnetic Field*, J. E. T. Channell, D. V. Kent, W. Lowrie, J. G. Meert, Eds. (American Geophysical Union, Washington, DC, 2004), pp. 255–265.
18. R. Muscheler, R. Beer, P. W. Kubik, H. A. Synal, *Quat. Sci. Rev.* **24**, 1849 (2005).
19. W. Broecker, S. Barker, *Earth Planet. Sci. Lett.* **256**, 90 (2007).
20. R. F. Anderson *et al.*, *Science* **323**, 1443 (2009).
21. P. Ciais *et al.*, *Nat. Geosci.* **5**, 74 (2012).
22. J. M. Yu *et al.*, *Science* **330**, 1084 (2010).
23. D. C. Lund, A. C. Mix, J. Southon, *Nat. Geosci.* **4**, 771 (2011).
24. L. Stott, J. Southon, A. Timmermann, A. Koutavas, *Paleoceanography* **24**, PA2223 (2009).
25. W. Broecker, E. Clark, *Geophys. Res. Lett.* **37**, L13606 (2010).
26. A. Burke, L. F. Robinson, *Science* **335**, 557 (2012).

27. E. Bard, F. Rostek, J. L. Turon, S. Gendreau, *Science* **289**, 1321 (2000).
28. T. Tschumi, F. Joos, M. Gehlen, C. Heinze, *Clim. Past* **7**, 771 (2011).
29. R. Zech, Y. Huang, M. Zech, R. Tarozo, W. Zech, *Clim. Past* **7**, 501 (2011).
30. N. Zeng, *Clim. Past* **3**, 135 (2007).
31. D. A. Hodell, C. D. Charles, F. J. Sierro, *Earth Planet. Sci. Lett.* **192**, 109 (2001).
32. B. Lemieux-Dudon *et al.*, *Quat. Sci. Rev.* **29**, 8 (2010).
33. North Greenland Ice Core Project members, *Nature* **431**, 147 (2004).
34. EPICA Community Members, *Nature* **444**, 195 (2006).
35. B. Stenni *et al.*, *Science* **293**, 2074 (2001).

Acknowledgments: We thank two anonymous reviewers for carefully reviewing the manuscript. Supported in part by Deutsche Forschungsgemeinschaft, Helmholtz Gemeinschaft, and Schweizerischer Nationalfonds. This work is a contribution to EPICA, a joint European Science Foundation/European Commission (EC) scientific program, funded by the EC under the Environment and Climate Program and by national contributions from Belgium, Denmark, France, Germany, Italy, the Netherlands, Norway, Sweden, Switzerland, and the UK. The main logistic support at Dome C was provided by the Institut Polaire Français–Paul Emile Victor (IPEV) and PNRA. Ice core material was also used from TALDICE, a joint European program led by Italy and funded by national contributions from Italy, France, Germany, Switzerland, and the UK. The main logistical support at Talos Dome was provided by PNRA. This is EPICA publication 284. The data are accessible online at http://doi.pangaea.de/10.1594/PANGAEA.772713.

Supplementary Materials
www.sciencemag.org/cgi/content/full/science.1217161/DC1
Materials and Methods
Figs. S1 to S7
Tables S1 to S3
References (*36*–*49*)

28 November 2011; accepted 19 March 2012
Published online 29 March 2012;
10.1126/science.1217161

Ancient Maya Astronomical Tables from Xultun, Guatemala

William A. Saturno,[1]* David Stuart,[2] Anthony F. Aveni,[3] Franco Rossi[4]

Maya astronomical tables are recognized in bark-paper books from the Late Postclassic period (1300 to 1521 C.E.), but Classic period (200 to 900 C.E.) precursors have not been found. In 2011, a small painted room was excavated at the extensive ancient Maya ruins of Xultun, Guatemala, dating to the early 9th century C.E. The walls and ceiling of the room are painted with several human figures. Two walls also display a large number of delicate black, red, and incised hieroglyphs. Many of these hieroglyphs are calendrical in nature and relate astronomical computations, including at least two tables concerning the movement of the Moon, and perhaps Mars and Venus. These apparently represent early astronomical tables and may shed light on the later books.

The Maya have long been noted for their astronomical proficiency, believed by many to be on par with that of the cultures of the ancient Middle East. Most of what we know about Maya astronomical methodology, and the precision of their understanding of the movement of the Sun, Moon, and planets, comes from studies of the codices, painted bark paper documents dated to a century or two before Spanish contact. Here we report on a source several centuries earlier, a wall painting accompanied by a numerical table and a series of long numbers that appear to have functioned like those found in astronomical tables in the codices.

Though systematic archaeological investigations began only in 2008 (*1*), the Maya ruins of Xultun, Guatemala, were first reported in 1915 (*2*). Despite formal scientific expeditions to map and record the site's monuments in the 1920s (*2*) and again in the 1970s (*3, 4*), illicit excavations have left the largest mark on the site. In March 2010, Maxwell Chamberlain identified the presence of a heavily eroded mural painting on the west wall of a small masonry-vaulted structure exposed by looting (*5*). The structure (Fig. 1), designated 10K-2, is located within a residential compound and was modified by the Maya over several construction phases. The most recent of these phases saw the room filled with rubble and earth, and the final phase built over it, effectively preserving its interior paintings. The looters' excavation broke through this final-phase veneer and exposed the southernmost portion of the room's west wall. They later abandoned their excavation, and the exposed painting began to weather.

We continued excavating this structure in 2010 and 2011, revealing that three of the structure's interior walls (west, north, and east), as well as its vaulted ceiling, were once covered by mural paintings. The fourth (south) wall consisted mainly of a doorway, with the remainder destroyed by the looters. The state of preservation of the murals varies considerably, owing to the damaging effects of water, roots, and insects. The east wall, located closest to the exterior surface of the covering mound, has eroded the most.

The paintings on the east wall include a large number of small, delicately painted hieroglyphs, rendered in a variety of sizes and in black or red line near the two (possibly three) seated figures that once dominated the imagery. Thin coats of plaster were reapplied over existing texts to provide a clean slate for others. Still other texts are incised into the plaster surface. Given their arrangement around and on the figural painting and

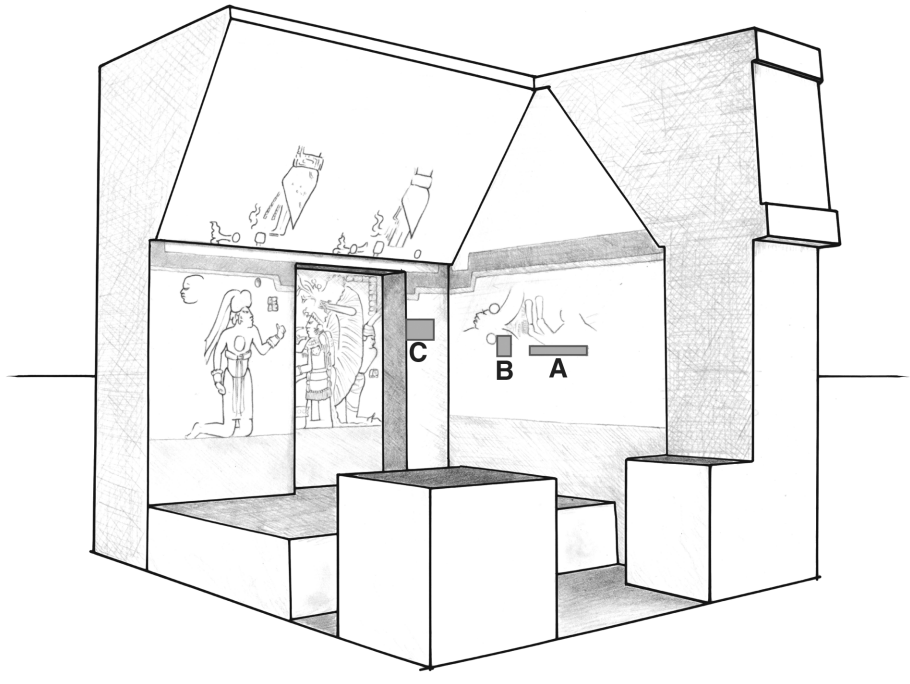

Fig. 1. Artist's reconstruction of Structure 10K-2, Xultun, Guatemala, showing painted figures from the north and east walls, as well as the locations of numerical arrays discussed in the text. (**A**) Lunar table. (**B**) "Ring Number." (**C**) Intervals. [Drawing by H. Hurst]

[1]Archaeology Department, Boston University, Boston, MA 02215, USA. [2]Department of Art and Art History, University of Texas at Austin, Austin, TX 78712, USA [3]Department of Physics and Astronomy, Department of Sociology and Anthropology, Colgate University, Hamilton, NY 13346, USA. [4]Archaeology Department, Boston University, Boston, MA 02215, USA.

*To whom correspondence should be addressed. E-mail: saturno@bu.edu